

Nonlinear fast-slow dynamics of a coupled fractional order hydropower generation system

Xiang Gao(高翔), Diyi Chen(陈帝伊), Hao Zhang(张浩), Beibei Xu(许贝贝), Xiangyu Wang(王翔宇)

Citation: Chin. Phys. B . 2018, 27(12): 128202. **doi:** 10.1088/1674-1056/27/12/128202
Journal homepage: http://cpb.iphy.ac.cn; http://iopscience.iop.org/cpb

What follows is a list of articles you may be interested in

A novel multi-scroll chaotic generator: Analysis, simulation, and implementation

Gui-Tao Zhang(张桂韬), Fa-Qiang Wang(王发强)

Chin. Phys. B . 2018, 27(1): 018201. **doi:** 10.1088/1674-1056/27/1/018201

Bursting oscillations in a hydro-turbine governing system with two time scales

Qing-Shuang Han(韩青爽), Di-Yi Chen(陈帝伊), Hao Zhang(张浩)

Chin. Phys. B . 2017, 26(12): 128202. **doi:** 10.1088/1674-1056/26/12/128202

Numerical simulation and analysis of complex patterns in a two-layer coupled reaction diffusion system

Li Xin-Zheng, Bai Zhan-Guo, Li Yan, He Ya-Feng, Zhao Kun

Chin. Phys. B . 2015, 24(4): 048201. **doi:** 10.1088/1674-1056/24/4/048201

Nonlinear dynamic characteristics and optimal control of a giant magnetostrictive film-shaped memory alloy composite plate subjected to in-plane stochastic excitation

Zhu Zhi-Wen, Zhang Qing-Xin, Xu Jia

Chin. Phys. B . 2014, 23(8): 088201. **doi:** 10.1088/1674-1056/23/8/088201

A voltage-controlled chaotic oscillator based on carbon nanotube field-effect transistor for low-power embedded systems

Van Ha Nguyen, Wonkyeong Park, Namtae Kim, Hanjung Song

Chin. Phys. B . 2014, 23(5): 058201. **doi:** 10.1088/1674-1056/23/5/058201

Nonlinear fast–slow dynamics of a coupled fractional order hydropower generation system*

Xiang Gao(高翔)[1,2], Diyi Chen(陈帝伊)[1,2,3,†], Hao Zhang(张浩)[1,2], Beibei Xu(许贝贝)[1,2], and Xiangyu Wang(王翔宇)[3]

[1] *Key Laboratory of Agricultural Soil and Water Engineering in Arid and Semiarid Areas, Ministry of Education, Northwest A & F University, Yangling* 712100, *China*

[2] *Institute of Water Resources and Hydropower Research, Northwest A & F University, Yangling* 712100, *China*

[3] *Australasian Joint Research Centre for Building Information Modelling, School of Built Environment, Curtin University, WA* 6102, *Australia*

(Received 18 May 2018; revised manuscript received 9 October 2018; published online 10 November 2018)

Internal effects of the dynamic behaviors and nonlinear characteristics of a coupled fractional order hydropower generation system (HGS) are analyzed. A mathematical model of hydro-turbine governing system (HTGS) with rigid water hammer and hydro-turbine generator unit (HTGU) with fractional order damping forces are proposed. Based on Lagrange equations, a coupled fractional order HGS is established. Considering the dynamic transfer coefficient *e*is variational during the operation, introduced *e* as a periodic excitation into the HGS. The internal relationship of the dynamic behaviors between HTGS and HTGU is analyzed under different parameter values and fractional order. The results show obvious fast–slow dynamic behaviors in the HGS, causing corresponding vibration of the system, and some remarkable evolution phenomena take place with the changing of the periodic excitation parameter values.

Keywords: fast–slow dynamics, fractional order, nonlinear dynamics, hydropower generation system

PACS: 82.40.Bj, 88.60.K–, 88.40.fc **DOI:** 10.1088/1674-1056/27/12/128202

1. Introduction

Due to the hydro-mechanical-electric coupling characteristics of the hydropower station system, there are a wide variety of complex nonlinear dynamic behaviors in the operation.[1] As two core parts of the hydropower station, the nonlinear analysis of the hydro-turbine governing system (HTGS) and hydro-turbine generator unit (HTGU) has attracted wide interest from scholars.[2–9] The development of the nonlinear theory and the introduction of the fractional order makes analysis on the nonlinear behaviors more diverse.[10–20] Related researches gradually evolved from the single subsystem to the internal connection of overall system.

Former correlational researches on the hydropower station system mainly focus on the model optimization and the stability control.[21] Researches on HTGS investigated the dynamics of the hydropower system by an accurate model that is based on the practical hydropower station and introduction of other physics phenomena such as time-delay.[5,22–24] In addition, developments of various control methods, such as sliding mode control and fuzzy logic control, are applied to the stability control of hydro-turbine governing system.[25] For the HTGU, shaft vibration and the description of multiple complex forces are emphasized in the majority studies. The vibration problem directly affects the stable operation and efficiency of the hydropower station.[26]

Although a lot of results have been made in the HTGS and HTGU, few studies have examined the internal effects of the dynamic phenomena in HGS. As a hydro-mechanical–electric coupled system, there is a tight link between each component. Therefore, an overall analysis of the system dynamics can give a more complete picture of the interaction in HGS, as well as the mechanism of various dynamic behaviors.

In light of this, this paper proposed a fractional order HGS model constituted with the HTGS and HTGU to analyze the dynamic characteristics in detail. First, mathematical models of HTGS with rigid water hammer and HTGU with fractional order damping forces are established. According to the Lagrange theory, coupling the HTGS and HTGU to get the coupled fractional order HGS. Because the transfer coefficient *e* changes during the operation, *e* is introduced into the HGS model as a periodic excitation. The internal effect in HGS is obtained by comparing the dynamic behaviors of rotational speed and shaft vibration. Meanwhile, effects of fractional order on the changes of the HGS behaviors are analyzed. Finally, the bifurcation diagram of the HGS shows the evolution characteristics of the dynamic behaviors of the HGS under different excitation parameter values.

The rest of this paper is organized as follows. In Sec-

*Project supported by the National Natural Science Foundation of China for Outstanding Youth (Grant No. 51622906), the National Natural Science Foundation of China (Grant No. 51479173), the Fundamental Research Funds for the Central Universities (Grant No. 201304030577), the Scientific Research Funds of Northwest A & F University (Grant No. 2013BSJJ095), and the Science Fund for Excellent Young Scholars from Northwest A & F University and Shaanxi Nova Program, China (Grant No. 2016KJXX-55).

†Corresponding author. E-mail: diyichen@nwsuaf.edu.cn

© 2018 Chinese Physical Society and IOP Publishing Ltd

tion 2, the coupled fractional order HGS model is derived. In Section 3, the results of numerical simulations are discussed from two aspects. The dynamic behaviors under different periodic parameter values are discussed, and the HGS stability under different dynamics are analyzed. Our concluding remarks and the future work are provided in Section 4.

2. Modeling

2.1. HTGS

The hydro-turbine used in this paper is a Francis turbine. The relationship between the hydro-turbine torque and the output power in the dynamic model of the hydro-turbine and water diversion system is

$$P_{\mathrm{m}} = m_{\mathrm{t}} + n, \tag{1}$$

where P_{m}, m_{t}, and n are the relative division of the output power, hydro-turbine torque, and rotational speed.

The transfer function is

$$G_{\mathrm{t}}(s) = e_y \frac{1 + eG_{\mathrm{h}}(s)}{1 - e_{\mathrm{qh}} G_{\mathrm{h}}(s)}, \tag{2}$$

where $G_{\mathrm{h}}(s)$ is the transfer function of the conduit system, e is the intermediate variable, e_y and e_{qh} are the transfer coefficient of the servomotor and water head.

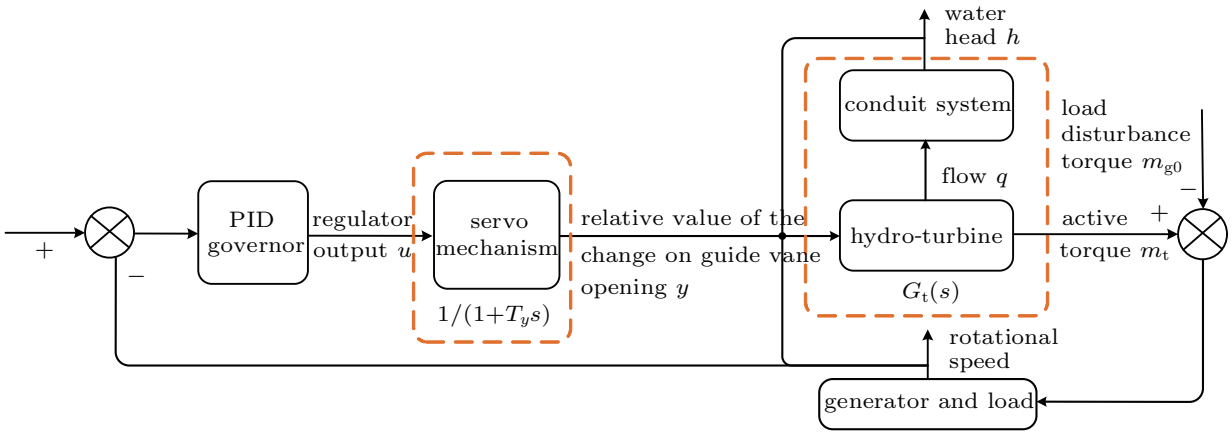


Fig. 1. (color online) Structure chart of the hydro-turbine governing system (HTGS).

From Fig. 1, the output torque of the hydro-turbine with rigid water hammer can be written as

$$\dot{m}_{\mathrm{t}} = \frac{1}{e_{\mathrm{qh}} T_{\mathrm{w}}} \left[-m_{\mathrm{t}} + e_y y - \frac{e e_y T_{\mathrm{w}}}{T_y} \left(u - y_{\mathrm{g}} \right) \right]. \tag{3}$$

where m_{t} and y_{g} are the relative values of the output torque and the guide vane opening, T_y and T_{w} are the inertial time constants of the servomotor and the water in the diversion system, u is the regulator output.

The nonlinear model of a second order generator is

$$\begin{aligned} \dot{\delta} &= \omega_0 n, \\ \dot{n} &= \frac{1}{T_{\mathrm{ab}}} \left[m_{\mathrm{t}} - m_{\mathrm{e}} - Dn \right], \end{aligned} \tag{4}$$

where D and T_{ab} are the hydro-turbine damping coefficient and inertial time constants, m_{e} is the electromagnetic torque.

The electromagnetic power is

$$P_{\mathrm{e}} = \frac{E'_{\mathrm{q}} V_{\mathrm{s}}}{x'_{\mathrm{d}\Sigma}} \sin\delta + \frac{V_{\mathrm{s}}^2}{2} \frac{x'_{\mathrm{d}\Sigma} - x_{\mathrm{q}\Sigma}}{x'_{\mathrm{d}\Sigma} x_{\mathrm{q}\Sigma}} \sin 2\delta, \tag{5}$$

where E'_{q} is the electric potential, V_{s} is the infinite busbar voltage.

2.2. HTGU

The changeability of the differential and integral order in the fractional calculus extends the dynamic descriptive ability of the commonly used integer order calculus. Especially for complex systems, since the dynamic process of the actual system is fractional, the fractional order can accurately describe the essential characteristics of the system and its dynamic behaviors. The fractional order damping forces acting on the HTG shaft in the stable operation can be written as

$$\begin{aligned} F_x &= cD^{\alpha} x, \\ F_y &= cD^{\alpha} y, \end{aligned} \tag{6}$$

where F_x and F_y are the damping forces on the x axis and y axis and c is the damping coefficient.

The fractional order model of the oil film forces can be described as

$$\begin{aligned} F_{x-\mathrm{off}} &= F_{x0-\mathrm{off}} + c_{xx} D^{\alpha} x + c_{xy} D^{\alpha} y + k_{xx} x + k_{xy} y, \\ F_{y-\mathrm{off}} &= F_{y0-\mathrm{off}} + c_{yx} D^{\alpha} x + c_{yy} D^{\alpha} y + k_{yx} x + k_{yy} y, \end{aligned} \tag{7}$$

where $F_{x0-\mathrm{off}}$ and $F_{y0-\mathrm{off}}$ are the oil-film forces at the quiescent operation point and the symbols k_{xx}, k_{xy}, k_{yx}, k_{yy}, c_{xx}, c_{xy}, c_{yx}, and c_{yy} are the linearized stiffness and damping coefficients.

The generator included in the HTG is composed by the rotor and the stator. When the rotor is moved rapidly relative

to the stator, the uneven air gap causes an asymmetric magnetic pull. When the generator has more than three pole pairs, the asymmetric magnetic pull can be described as

$$F_{x-\mathrm{ump}} = \frac{dL\pi k_{\mathrm{i}}^2 I_{\mathrm{i}}^2 (2v_0 v_1 + v_1 v_2 + v_2 v_3)\cos\lambda}{4\mu_0},$$
$$F_{y-\mathrm{ump}} = \frac{dL\pi k_{\mathrm{i}}^2 I_{\mathrm{i}}^2 (2v_0 v_1 + v_1 v_2 + v_2 v_3)\sin\lambda}{4\mu_0}, \quad (8)$$

where d is the radius of the rotor, L is the length of the generator rotor, μ_0 denotes the magnetic permeability of the air, k_{i} is the coefficient of magneto-motive force fundamental wave of the air gap, I_{i} represents the exciting current of the generator and v_0, v_1, v_2, and v_3 are intermediate variables.

From Fig. 2, we can obtain the relationship of the axis of the generator rotor and turbine runner

$$x_1 = x_2 - r\cos(\omega t + \theta_0),$$
$$y_1 = y_2 - r\sin(\omega t + \theta_0), \quad (9)$$

where x_1, y_1 and x_2, y_2 are the coordinates of the axis of the generator rotor and turbine runner, respectively, r is the eccentric distance, ω is the angular speed and θ_0 is the phase shift.

We have

$$x_{\mathrm{m1}} = x_1 + e_1\cos(\omega t + \varphi_0),$$
$$y_{\mathrm{m1}} = y_1 + r\sin(\omega t + \varphi_0),$$
$$x_{\mathrm{m2}} = x_2 + e_2\cos(\omega t + \varphi_0),$$
$$y_{\mathrm{m2}} = y_2 + r\sin(\omega t + \varphi_0), \quad (10)$$

where x_{m1}, y_{m1}, x_{m2}, and y_{m2} are the mass center of the generator rotor and the turbine runner, respectively, φ_0 is the initial phase of the generator rotor, and e_1 and e_2 denote the mass eccentricity of the generator and turbine.

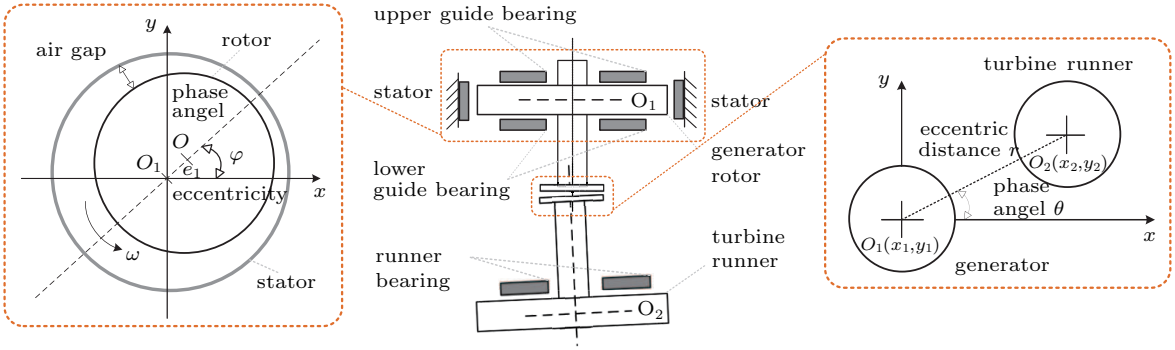


Fig. 2. (color online) Schematic diagrams of the shaft misalignment and generator air-gap eccentricity.

2.3. Coupled HGS modeling

Assuming that the static balance is the point of potential energy, the potential U and kinetic T energies of the shaft system can be described as

$$\begin{aligned} T &= T_1 + T_2, \\ T_1 &= \frac{1}{2}(J_1 + m_1 e_1^2)\dot{\varphi}^2 + \frac{1}{2}\left(J_2 + m_2(r^2 + e_2^2)\right)\dot{\theta}^2, \\ T_2 &= \frac{1}{2}m_1(\dot{x1}^2 + \dot{y}_1^2 + e_1^2\dot{\varphi}^2 - 2\dot{x1}e_1\dot{\varphi}\sin\varphi + 2\dot{y1}e_1\dot{\varphi}\cos\varphi) \\ &\quad + \frac{1}{2}m_2(\dot{x2}^2 + \dot{y}_2^2 + e_2^2\dot{\varphi}^2 - 2\dot{x2}e_2\dot{\varphi}\sin\varphi + 2\dot{y2}e_2\dot{\varphi}\cos\varphi), \\ U &= \frac{1}{2}k_1(x_1^2 + y_1^2) + \frac{1}{2}k_2(x_1^2 + y_1^2 \\ &\quad + 2rx_1\cos\theta + 2ry_1\sin\theta + r^2), \end{aligned} \quad (11)$$

where J_1 and J_2 are the rotary inertia of the generator rotor and turbine runner, m_1 and m_2 is the quality of the generator rotor and turbine runner, respectively, k_1 and k_2 are the stiffness of the rotor bearing and the turbine runner, respectively.

The Lagrange equations of the hydraulic turbine generator shaft system are

$$\frac{\mathrm{d}}{\mathrm{d}t}\left(\frac{\partial L}{\partial \dot{x}_1}\right) - \frac{\partial L}{\partial x_1} = \Sigma F_x,$$
$$\frac{\mathrm{d}}{\mathrm{d}t}\left(\frac{\partial L}{\partial \dot{y}_1}\right) - \frac{\partial L}{\partial y_1} = \Sigma F_y,$$
$$\frac{\mathrm{d}}{\mathrm{d}t}\left(\frac{\partial L}{\partial \omega}\right) - \frac{\partial L}{\partial \varphi} = M_{\mathrm{t}} - M_{\mathrm{g}}, \quad (12)$$

where M_{t} is the hydro-turbine torque, M_{g} is the generator magnetic torque and

$$M_{\mathrm{t}} - M_{\mathrm{g}} = \left(m_{\mathrm{t}} - m_{\mathrm{g}}\right) M_{\mathrm{gB}}. \quad (13)$$

Then, we obtain

$$\dot{\omega} = \left(B + M_{\mathrm{t}} - M_{\mathrm{g}}\right)/A, \quad (14)$$

where

$$\begin{aligned} A &= J_1 + J_2 + 2m_1 e_1^2 + 2m_2 e_2^2 + 2m_2 r^2 \\ &\quad + 2m_2 e_2 r\cos(\theta_0 - \varphi_0) \\ &\quad - \frac{1}{m_1 + m_2}\left\{\left[(m_1 e_1 + m_2 e_2)\sin\varphi + m_2 r\sin\theta\right]^2\right. \\ &\quad \left. + \left[(m_1 e_1 + m_2 e_2)\cos\varphi + m_2 r\cos\theta\right]^2\right\}, \end{aligned} \quad (15)$$

and

$$\begin{aligned} B &= \frac{\left[(m_1 e_1 + m_2 e_2)\sin\varphi + m_2 r\sin\theta\right]}{m_1 + m_2} \\ &\quad \times\left\{\left[(m_1 e_1 + m_2 e_2)\cos\varphi + m_2 r\cos\theta\right]\omega^2 - (k_1 + k_2)x_1\right. \end{aligned}$$

$$
\begin{aligned}
&-k_2 r\cos\theta + F_{x-\mathrm{ump}} + F_{x-\mathrm{off}} - F_x f\big\}\\
&-\frac{[(m_1e_1+m_2e_2)\cos\varphi - m_2 r\cos\theta]}{m_1+m_2}\\
&\times\big\{[(m_1e_1+m_2e_2)\sin\varphi + m_2 r\sin\theta]\,\omega^2 - (k_1+k_2)\,y_1\\
&-k_2 r\sin\theta + F_{y-\mathrm{ump}} + F_{y-\mathrm{off}} - F_y f\big\}\\
&+k_2 r(x_1\sin\theta - y_1\cos\theta). \qquad (16)
\end{aligned}
$$

Besides, the relationship between the relative deviation of the angular speed and the angular speed is

$$\dot{\omega} = \omega_{\mathrm{B}}\dot{n}, \qquad (17)$$

where ω_{B} is the standard value of the angular speed.

From the above equations, the coupled fractional model of the HGS can be written as

$$
\begin{aligned}
\dot{\delta} &= \omega_0\omega,\\
\dot{m}_{\mathrm{t}} &= \frac{1}{e_{\mathrm{qh}}T_{\mathrm{w}}}\Big[-m_{\mathrm{t}} + e_y y_{\mathrm{g}} - \frac{e e_y T_{\mathrm{w}}}{T_y}\\
&\quad\times\left(-k_{\mathrm{p}}\omega - k_{\mathrm{i}}\delta/\omega_0 - k_{\mathrm{d}}\dot{\omega} - y_{\mathrm{g}}\right)\Big],\\
\dot{y}_{\mathrm{g}} &= \frac{1}{T_y}\left(-k_{\mathrm{p}}\omega - k_{\mathrm{i}}\delta/\omega_0 - k_{\mathrm{d}}\dot{\omega} - y_{\mathrm{g}}\right),\\
\dot{n} &= \frac{B + M_{\mathrm{gB}}\left(m_{\mathrm{t}} - \frac{E_{\mathrm{q}}V_{\mathrm{s}}}{x'_{\mathrm{d}\Sigma}}\sin\delta - \frac{V_{\mathrm{s}}^2}{2}\frac{x'_{\mathrm{d}\Sigma}-x_{\mathrm{d}\Sigma}}{x'_{\mathrm{d}\Sigma}x_{\mathrm{d}\Sigma}}\sin 2\delta\right)}{A\omega_B},
\end{aligned}
$$

$$
\begin{aligned}
D^{\alpha}x &= v_x,\\
D^{\alpha}y &= v_y,\\
D^{2-\alpha}v_x &= \frac{1}{m_1+m_2}\big[-cv_x - (k_1+k_2)x\\
&\quad+(m_1e_1+m_2e_2)\omega^2\cos\varphi + (m_2\omega^2 - k_2)\cos\theta\\
&\quad+F_{x-\mathrm{ump}} + F_{x-\mathrm{off}}\big],\\
D^{2-\alpha}v_y &= \frac{1}{m_1+m_2}\big[-cv_y - (k_1+k_2)y\\
&\quad+(m_1e_1+m_2e_2)\omega^2\sin\varphi + (m_2\omega^2 - k_2)\sin\theta\\
&\quad+F_{y-\mathrm{ump}} + F_{y-\mathrm{off}}\big]. \qquad (18)
\end{aligned}
$$

3. Numerical simulation

The intermediate variable e, as a transfer coefficient in the HTGS, is always changing with the operating condition. To study the effect of this variability of e on the dynamic characteristics of the HGS, introducing e as a periodic excitation into the HGS model, and the equation of e is

$$e = A\times\cos(\Omega t), \qquad (19)$$

where A and Ω are the amplitude and frequency of the periodic excitation.

The parameters values and initial values of the HGS variables are shown in Table 1 and Table 2.

Table 1. Parameters values.

Parameters	Values	Units	Parameters	Values	Units
Mass of the rotor m_1	$1.6\cdot10^4$	kg	Eccentric distance r	$6\cdot10^{-4}$	m
Mass of the runner m_2	$12.3\cdot10^4$	kg	Damping coefficient c	$8.5\cdot10^5$	Ns/m
Bearing stiffness of the rotor k_1	$8.5\cdot10^7$	N/m	Magnetic permeability of the air μ_0	$4\pi\cdot10^{-7}$	H/m
Bearing stiffness of the runner k_2	$6.5\cdot10^7$	N/m	Initial phase θ_0	1	rad/s
Length of the rotor L	0.5	m	Initial phase φ_0	0.8	rad/s
Eccentric mass of the rotor e_1	$5\cdot10^{-4}$	kg	Initial value of angular speed ω_0	314	rad/s
Eccentric mass of the runner e_2	$5\cdot10^{-4}$	kg	Standard value of the angular speed ω_{B}	38	rad/s
Water head transfer coefficient e_{qh}	0.56	p.u.	Infinite busbar voltage V_{s}	1	p.u.
Damping coefficient D	2	p.u.	Inertial time constants T_{ab}	9	p.u.
Direct axis transient reactance x'_{d}	1.15	p.u.	Quartered axis reactance x_{q}	1.47	p.u.
Servomotor inertial time constants T_y	0.21	p.u.	Water inertial time constants T_{w}	0.8	p.u.
Electric potential E'_{q}	1.35	p.u.	Servomotor transfer coefficient e_y	1	p.u.

Table 2. Initial values of the HGS variables for the simulation.

HGS Variables	Initial values
Rotor angle δ	0.001
Relative values of the output torque m_{t}	0.001
Relative values of the guide vane opening y_{g}	0.001
Relative values of the rotational speed n	0.001
Coordinates of the x-axis x	0.00001
Coordinates of the y-axis y	0.00001
Accelerated speed of the x-axis v_x	0
Accelerated speed of the y-axis v_y	0

3.1. Dynamic behaviors

In this section, the effect of the periodic excitation e on the dynamic characteristics of the HGS is investigated. Considering the influence of different frequency of e, taking four sets of different frequency e to simulate the HGS dynamic behaviors. The basic value of e, *i.e.*, the amplitude of the excitation $A = 1.1$ in this paper and PID controller parameter values are $k_{\mathrm{p}} = 2.7$, $k_{\mathrm{i}} = 1$, and $k_{\mathrm{d}} = 1.5$, and four sets e frequency are 1, 0.1, 0.01, and 0.001. Four sets dynamic behaviors of the relative value of rotational speed n and displacement of x axis are shown in Fig. 3.

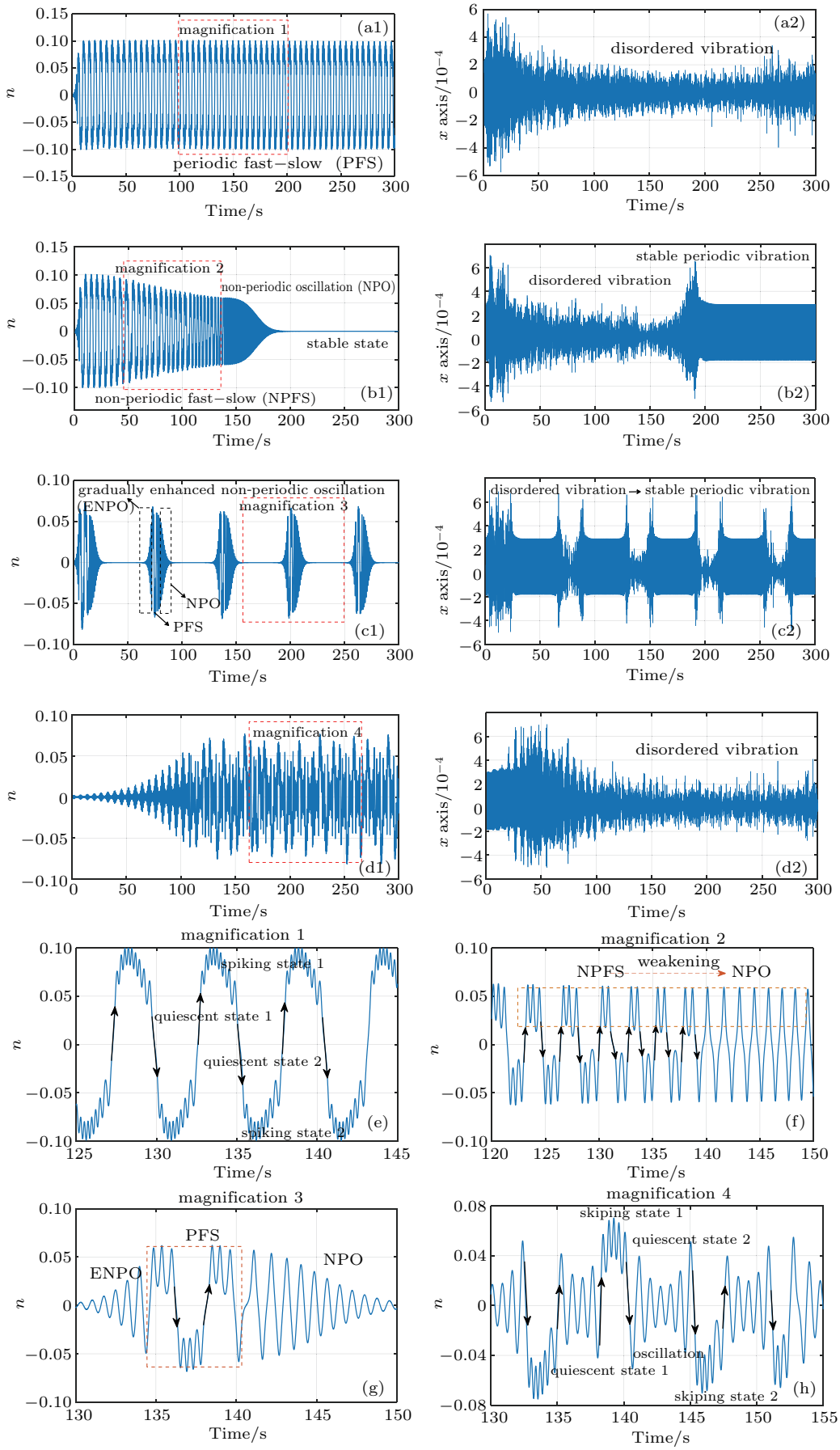


Fig. 3. (color online) The time waveforms of the rotational speed n and displacement of the x axis (a1) and (a2) $\Omega = 0.001$; (b1) and (b2) $\Omega = 0.01$; (c1) and (c2) $\Omega = 0.1$; (d1) and (d2) $\Omega = 1$.

From Fig. 3, the periodic excitation has significant effect on the dynamic behaviors of the HGS, and the dynamics phenomena have obvious difference under different e frequency. Periodic fast–slow dynamics (PFS) appears as an alternating transition from the quiescent state to the spiking state.[27,28] As shown in Figs. 3(a1) and 3(a2) and magnification Fig. 3(e), n shows obvious periodic fast–slow dynamics when $\Omega = 0.001$. Meanwhile, the displacement of the x axis shows disordered vibration when n is under PFS effects. The fast–slow effect accused by the different scale between the natural frequency and the excitation frequency. Spiking state is in the fast timescale, which refers to the concentrative field of the fast changing trajectory in the time history, and the trajectory connecting the spiking states corresponds to the quiescent state.

When $\Omega = 0.01$, the dynamic behaviors of n transitions from the non-periodic fast–slow state (NPFS) to the non-periodic oscillation state (NPO) and finally to the stable state. From magnification 2 (Fig. 3(f)), the spiking state of the fast–slow phenomenon gradually weakens until it enters the NPO. When n at the NPO and NPFS, x axis shows disordered vibration, and enters the stable periodic vibration state when n enters stable state.

When $\Omega = 0.1$, n shows periodic motion from ENPO (gradually enhanced NPO) to PFS to NPO to stable state. From magnification 3 (Fig. 3(g)), the dynamic behaviors of n directly transition from the PFS to the NPO instead of the NPFS weakening to the NPO. Under this kind of effect, the displacement of the x axis shows periodic alternating transition from the disordered vibration state to the stable periodic vibration state.

When $\Omega = 1$, a new fast–slow effect appears that n transition from the quiescent state 1 to the spiking state 1 to the quiescent state 2 to an oscillation state and then to the spiking state 2, as shown in magnification 4 (Fig. 3(h)). The displacement of x axis shows the same disordered vibration as $\Omega = 0.001$.

From this analysis, it can be seen that the periodic excitation has an obvious fast–slow effect on the HGS dynamics, and there is significant difference of the dynamic behaviors under different frequency of the periodic excitation. The PFS, NPFS, NPO, and stable state alternately transformed each other with the change of the e. Meanwhile, the dynamic behaviors of the displacement of x axis correspondingly changes with n. For the further analysis of the fast–slow effect, the phase diagrams of n versus rotor angle δ are shown in Fig. 4.

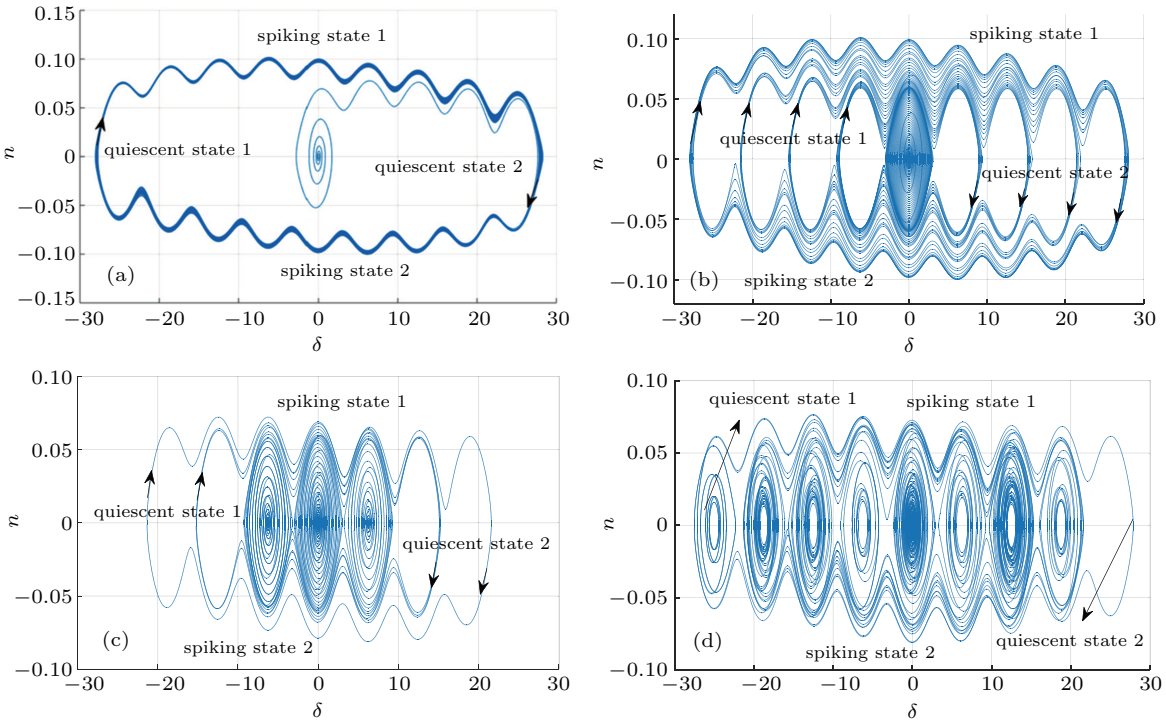


Fig. 4. (color online) The phase diagrams of the rotational speed n versus rotor angle δ. (a) $\Omega = 0.001$; (b) $\Omega = 0.01$; (c) $\Omega = 0.1$; (d) $\Omega = 1$.

From Fig. 4, the phase trajectories show obvious fast–slow dynamics phenomena, there is big difference under different excitation frequency. Figure 4(a) shows standard fast–slow dynamics phase trajectory that is an alternating transition process from quiescent state 1 to spiking state 1 to quiescent state 2 to spiking state 2. When $\Omega = 0.01$, consistent with the time waveforms, the phase trajectory shows different scale fast–slow phenomena and gradually enters the NPO state. Due to the small scale PFS when $\Omega = 0.1$, the major part of the phase trajectory shows the NPO and stable state. When $\Omega = 1$,

the phase trajectory shows the cross transitions of the spiking state, quiescent state and the oscillation state.

3.2. Fractional order effect

The fractional order damping forces are more accurate than the integer order in the description of the dynamic behaviors of the vibration system. To analyze the effect of the fractional order on the dynamic characteristics of the HGS, the x axis responses under different fractional order are shown in Fig. 5.

From Fig. 5, when $\Omega = 0.001$ and 1, the dynamic responses of x axis are in the disordered vibration state affected by PFS, ENPO, and NPO ($\Omega = 1$). As the increase of the fractional order, the amplitude of the disordered vibration gradually enhanced, and this phenomenon is more noticeable when the fractional order increases to 1. When $\Omega = 0.01$ and 0.1, the x-axis state is alternating transforming from disordered vibration to stable periodic vibration. The stable periodic vibration states experience almost no change with the increase of the fractional order, while the amplitude of the disordered vibration states are enhanced. It is worth noting that the degree of amplitude enhancement at the two state transitions are more pronounced.

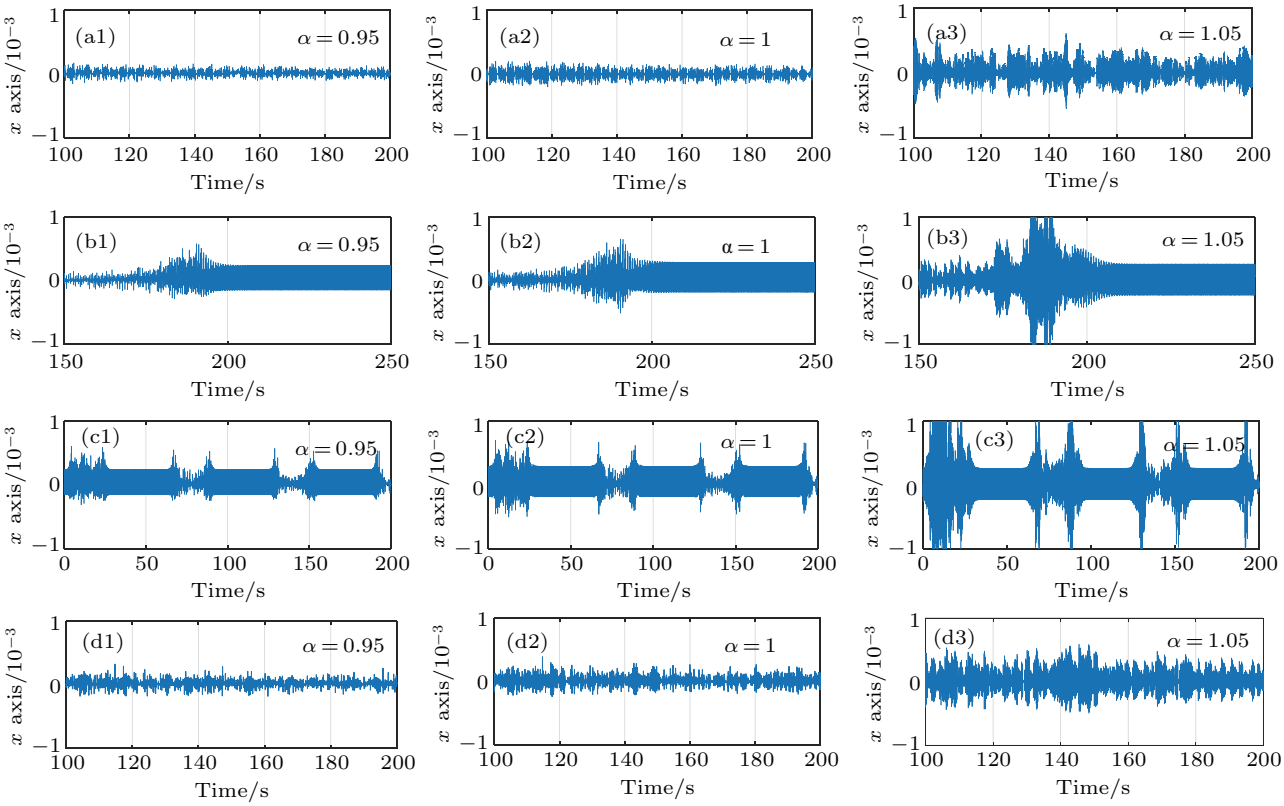


Fig. 5. (color online) Dynamic responses of the x-axis under different fractional orders. (a1)–(a3) $\Omega = 0.001$; (b1)–(b3) $\Omega = 0.01$; (c1)–(c3) $\Omega = 0.1$; (d1)–(d3) $\Omega = 1$.

3.3. Bifurcation characteristics

The introduction of the periodic excitation into the intermediate variable e has a significant effect on the dynamic behaviors of the HGS. Meanwhile, the difference of excitation parameter values caused diverse dynamic phenomena. To further analyze the effect of the periodic excitation on the stability of the HGS, the bifurcation diagrams of the rotational speed n with increase of the periodic excitation frequency Ω are shown in Fig. 6.

As shown in Fig. 6(a), the bifurcation of n has significantly evolution characteristic with the increase of the frequency Ω, and there are three key parts in the evolution process. First, as shown in Figs. 6(b)–6(c), n is converted from two clusters of symmetrical bifurcations into a cluster of convergent bifurcations that finally enter stable state. When $\Omega > 0.16$, the bifurcation behaviors of n enter an attenuation bifurcation cluster with obvious fluctuation rules. It worth noting that when Ω is around 0.34, the wave trough of the fluctuating bifurcation clusters overlapped makes this point close to the stable state. As shown in Fig. 6(f), when the $\Omega > 1$, the bifurcation behaviors enter the chaos state, and the degree of the chaos gradually decrease. The slow-fast dynamics has significant effects on the system stability, meanwhile, the effect degree is related to the state of the slow-fast behaviors caused by the different frequency of e.

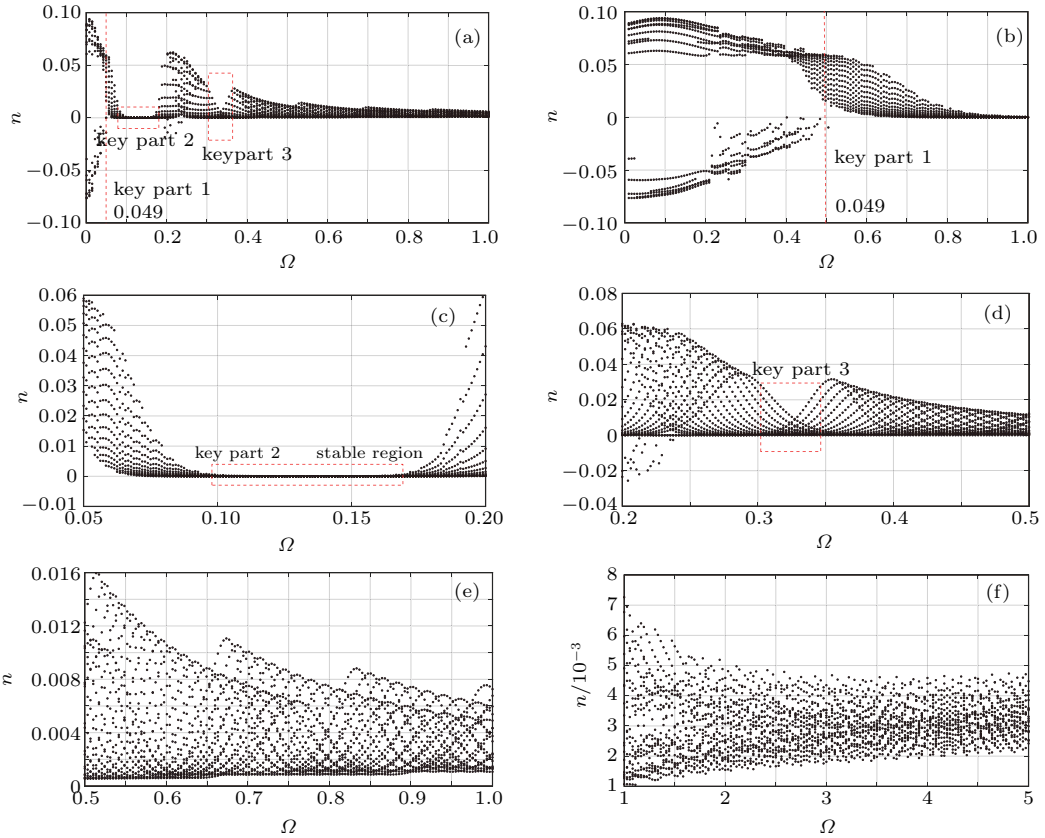


Fig. 6. (color online) The bifurcation diagrams of the rotational speed n with increase of the periodic excitation frequency Ω. (a) Ω from 0.01 to 1; (b) Ω from 0.01 to 0.1; (c) Ω from 0.05 to 0.2; (d) Ω from 0.2 to 0.5; (e) Ω from 0.5 to 1; (f) Ω from 1 to 5.

4. Conclusions

In this work, a fractional order model of HGS is presented, coupled by the HTGS with rigid water hammer and HTGU with fractional order damping forces. To describe the effect of the dynamic transfer coefficients e on the HGS accurately, the periodic excitation is introduced in to the HGS. Dynamic behaviors, effects of the fractional order and the evolution characteristics are analyzed in detail.

Obvious fast–slow dynamic phenomena are found in the process and multiple dynamic behaviors alternately transform each other as the periodic excitation frequency changes. Fast–slow dynamic behaviors caused corresponding disordered vibration on the shaft. Fractional order changes have little effect on the stable dynamic behaviors of the x axis, while they have the greatest impact on the junction points of unstable and stable states, causing larger vibration amplitude. Moreover, the HGS bifurcation behaviors shows an evolution trend from bifurcation to chaos with the increase of the excitation frequency and some interesting phenomena take place in the process.

References

[1] Sarasúa J I, Pérez-Díaz J I, Wilhelmi J R and Á J 2015 *Energy Conv. Manag.* **106** 151
[2] Zeng Y, Zhang L X, Guo Y K, Qian J and Zhang C L 2014 *Nonlinear Dyn.* **76** 1921
[3] Zeng Y, Zhang L X, Guo Y K and Qian J 2015 *Int. J. Control Autom* **13** 867
[4] Joseph A, Desingu K, Semwal R R, Chelliah T R and Khare D 2017 *IEEE T. Energy Conver.* **33** 430
[5] Mesnage H, Alamir M, Perrissin-Fabert N and Alloin Q 2017 *Eur. J. Ccontrol* **34** 24
[6] Moradi H, Alasty A and Vossoughi G 2013 *Energy Conv. Manag.* **68** 105
[7] Pico H V, Mccalley J D, Angel A, Leon R and Castrillon N J 2012 *IEEE T. Power Syst.* **27** 1906
[8] Michelsen F A, Wilhelmsen Ø Zhao L and Åsen K I 2013 *Energy Conv. Manag.* **67** 160
[9] Poirier M, Gagnon M, Tahan A, Coutu A and Chamberland-Lauzon J 2017 *Mech. Syst. Signal Pr.* **82** 193
[10] Alexopoulos A and Weinberg G V 2014 *Phys. Lett. A* **378** 2478
[11] Li W, Zhang M T and Zhao J F 2017 *Chin. Phys. B* **26** 090501
[12] Bardeji S G, Figueiredo I N and Sousa E 2017 *Appl. Num. Math.* **114** 188
[13] Izsák F and Szekeres B J 2017 *Appl. Math. Lett.* **71** 38
[14] Jothiprakash V, Arunkumar R 2013 *Water Resour. Manag.* **27** 1963
[15] Layek G C and Pati N C 2017 *Phys. Lett. A* **381** 3568
[16] Kumar S, Kumar D and Singh J 2016 *Adv. Nonlinear Anal.* **5** 383
[17] Andrew L Y T, Li X F, Chu Y D and Zhang H 2015 *Chin. Phys. B* **24** 100520
[18] Pahnehkolaei S M A , Alfi A and Machado J A T 2017 *Commun. Nonlinear Sci. Num. Simul.* **47** 328
[19] Sakaguchi H and Okita T 2016 *Phys. Rev. E* **93** 022212
[20] Ma J H and Ren W B 2016 *Int. J. Bifur. Chaos* **26** 1650181
[21] Li H H, Chen D Y, Zhang H, Wang F F and Ba D D 2016 *Mech. Syst. Signal Proc.* **80** 414
[22] Xu B B, Chen D Y, Tolo S, Patelli E and Jiang Y L 2018 *Int. J. Elec. Power* **95** 156
[23] Si G Q, Diao L J, Zhu J W, Lei Y H and Zhang Y B 2017 *Chin. Phys. B* **26** 060503
[24] Li H H, Chen D Y, Xu B B, Tolo S and Patelli E 2017 *Nonlinear Dyn.* **90** 535
[25] Mandić P D, T B Š Lazarević M P and Bošković M 2017 *ISA T.* **67** 76
[26] Pay S S 2016 *Chin. Phys. B* **25** 040204
[27] Xu B B, Chen D Y, Zhang H and Zhou R 2015 *Nonlinear Dyn.* **81** 1263
[28] Xu B B, Chen D Y, Behrens P, Ye W, Guo P C and Luo X Q 2018 *Energy Conv. Manag.* **174** 208